

1 Natural new particle formation at the coastal Antarctic site 2 Neumayer

3
4 R. Weller¹, K. Schmidt¹, K. Teinilä², and R. Hillamo²

5
6 [1] Alfred Wegener Institute for Polar and Marine Research, Am Handelshafen 12, D-27570
7 Bremerhaven, Germany

8 [2] Finnish Meteorological Institute, Erik Palménin aukio 1, FI-00101 Helsinki, Finland

9 Correspondence to: R. Weller (rolf.weller@awi.de)

10

11 Abstract

12 We measured condensation particle (CP) concentrations and particle size distributions at the
13 coastal Antarctic station Neumayer (70°39'S, 8°15'W) during two summer campaigns (from
14 20 January to 26 March 2012 and 1 February to 30 April 2014) and during polar night
15 between 12 August and 27 September 2014 in the particle diameter (D_p) range from 2.94 nm
16 to 60.4 nm (2012) and from 6.26 nm to 212.9 nm (2014). During both summer campaigns we
17 identified all in all 44 new particle formation (NPF) events. From 10 NPF events, particle
18 growth rates could be determined to be around 0.90 ± 0.46 nm h⁻¹ (mean \pm std; range:
19 0.4 nm h⁻¹ to 1.9 nm h⁻¹). With the exception of one case, particle growth was generally
20 restricted to the nucleation mode ($D_p < 25$ nm) and the duration of NPF events was typically
21 around 6.0 ± 1.5 h (mean \pm std; range: 4 h to 9 h). **Thus in the surrounding area of Neumayer,**
22 **particles did not grow up to sizes required for acting as cloud condensation nuclei.** NPF
23 during summer usually occurred in the afternoon in coherence with local photochemistry.
24 During winter, two NPF events could be detected, though showing no ascertainable particle
25 growth. A simple estimation indicated that apart from sulfuric acid, the derived growth rates
26 required other low volatile precursor vapours.

27 1 Introduction

28 The crucial role of aerosols as a key component in governing radiation transfer through the
29 Earth's atmosphere and thus their pivotal role in determining climate, has boosted aerosol
30 research activities and strongly promoted our knowledge on this topic. Their relevance in
31 climate forcing is most notably evident since they potentially act as condensation nuclei for
32 cloud droplets, thus influencing radiation transfer indirectly (Haywood and Boucher, 2000;
33 Ramanathan et al., 2001; Carslaw et al., 2013; Rosenfeld et al., 2014). In particular due to the
34 latter effect, involving inherently complicated feedback mechanisms, aerosols still notoriously
35 contribute to the largest uncertainty in estimating climate forcing (for a comprehensive
36 treatise we refer to Boucher et al., 2013 and references therein).

37 One focus of interest in aerosol research is dedicated to questions regarding new particle
38 formation (NPF), the dominant global particle source generating so-called secondary aerosol
39 (Spracklen et al., 2006). This process starts with the nucleation of gaseous precursors to
40 molecular clusters (Zhang et al., 2012) followed by particle growth to sizes potentially
41 relevant for acting as cloud condensation nuclei (CCN; Spracklen et al., 2008; Bzdek and
42 Johnston, 2010).

43 Recent research activities documented the global importance of natural secondary aerosol
44 from the marine atmosphere and revealed that apart from dimethyl sulfide (DMS) derived
45 sulfuric acid (H_2SO_4), especially marine volatile organic compounds (VOC) but also reactive
46 iodine species mediate particle nucleation and growth (O'Dowd et al., 2002a and 2002b;
47 Henze and Seinfeld, 2006; O'Dowd and de Leeuw, 2007; Facchini et al., 2008a; McFiggans et
48 al., 2010). Notably in terms of secondary aerosol formation, the virtually completely ice
49 covered and thus effectively source free Antarctic continent represents an outstanding case:
50 Surrounded and isolated by the Southern Ocean from other continents, NPF should be
51 inherently linked with the advection of marine air masses. Apart from some earlier work
52 reporting on the frequent occurrence of bimodal particle size distributions below 100 nm in
53 coastal Antarctica (Ito, 1985 and 1993; Jaenicke et al., 1992), NPF has been recently
54 described for several Antarctic sites. Most extensive measurements were conducted at the

55 Finnish station Aboa (73°03'S, 13°25'W, 496 m a.s.l.), located on a nunatak about 130 km
56 from the sea (Koponen et al., 2003; Asmi et al., 2010, Kyrö et al., 2013). Asmi et al. (2010)
57 reported on NPF events showing growth rates (GR) within the nucleation mode between
58 0.8 nm h⁻¹ and 2.5 nm h⁻¹, while in a subsequent summer campaign, significantly higher GR
59 between 1.8 nm h⁻¹ and 8.8 nm h⁻¹ were found and particle growth usually extended well into
60 the Aitken mode (Kyrö et al., 2013). A thorough data analysis by Kyrö et al. (2013) revealed
61 that most probably biogenic precursors originating from local melting ponds provided low
62 volatile vapour needed for the observed particle growth. Hence this study was the first one
63 indicating that (biogenic) emissions from continental Antarctic could be a source for
64 secondary aerosol formation and relativized the source free character of continental
65 Antarctica. Regarding the Antarctic Plateau, NPF events reported from South Pole were
66 ascribed to local contamination (Park et al., 2004). In contrast, during year-round
67 measurements at Dome C (75°06'S, 123°23'E, 3200 m a.s.l.) several NPF events could be
68 observed throughout the year, mostly associated with particle growth starting from the
69 nucleation into the Aitken mode (Järvinen et al., 2013). Most surprisingly, growth rates
70 tentatively appeared even higher compared to Aboa (median considering all events:
71 2.5 nm h⁻¹, range: 0.5 nm h⁻¹ to 14.1 nm h⁻¹; Järvinen et al., 2013). Finally a recent ship-borne
72 study indicated a Hg driven nucleation event over East Antarctic sea ice (Humphries et al.,
73 2015). Complementary to these local field investigations, dedicated modelling studies can
74 give spatially inclusive and comprehensive insights regarding sources and mechanisms of
75 NPF and the influence on CCN concentrations in the remote atmosphere of the Southern
76 Ocean. Korhonen et al.'s (2008) work revealed a weaker impact of DMS derived secondary
77 aerosol on marine CCN concentrations at high southern latitudes, largely caused by much
78 stronger sea spray emissions south of 45°S. This study also emphasized the importance of
79 NPF in the free troposphere followed by particle growth during entrainment into the marine
80 boundary layer. Yu and Luo's (2010) investigations targeted on modelling DMS derived NPF
81 around coastal Antarctica and demonstrated that ion-mediated nucleation can reasonably
82 predict the observed seasonality of condensation particle (CP) concentrations at coastal
83 Antarctica.

84 Our present work ties in with a previous publication that examined the climatology of CP
85 concentrations at the German Antarctic research station Neumayer (Weller et al., 2011a). This
86 precedent study indicated the importance of particle nucleation occurring even during late
87 winter and early spring in determining particle number concentrations. In the current study we
88 will entirely focus on the dynamics of particle size distribution and NPF, relying on two
89 dedicated summer campaigns in 2012 and 2014, as well as a measuring period during austral
90 winter (August and September 2014).

91

92 **2 Experimental techniques and data evaluation methods**

93 **2.1 Site description and instrumentation**

94 All experiments were conducted inside the Air Chemistry Observatory located close to
95 Neumayer Station (NM, 70°39' S, 8°15'W, [http://www.awi.de/en/science/long-term-
96 observations/atmosphere/antarctic-neumayer/air-chemistry.html](http://www.awi.de/en/science/long-term-observations/atmosphere/antarctic-neumayer/air-chemistry.html), last access: 01 October
97 2015). Measuring site, prevailing local meteorological conditions, characteristics of the air
98 inlet system, and finally aspects of contamination free sampling have already been described
99 in some detail and we refer to König-Langlo et al. (1998) and Weller et al. (2011a and
100 references therein).

101 The size distribution of the sub- μm aerosol at NM was determined by a scanning mobility
102 particle sizer (SMPS, TSI classifier model 3080; Wang and Flagan, 1990). During austral
103 summer 2012, i.e. from 20 January through 26 March, the classifier was operated with a so-
104 called nano-DMA (nano differential mobility analyser, TSI Model 3085) in combination with
105 a condensation particle counter (CPC, TSI model WCPC 3788, 50% cut-off diameter $D_{p(50\%)}$
106 of 2.5 nm). We adjusted aerosol and sheath flow to achieve nominal aerosol size distribution
107 measurements **between 2 nm and 64 nm** with a 64 channel resolution. Note that the SMPS
108 primarily measured the electrical mobility of particles which was finally converted by a
109 known transfer function to the corresponding particle mobility diameter D_p . Due to increased
110 uncertainty caused by diffusional losses and cut-off corrections for the used CPC, we

111 evaluated the data starting from 3 nm. All size spectra were multiple charge and diffusion
 112 corrected according to the TSI software AIM (Aerosol Instrument Manager[®]). The original
 113 spectra were taken with a scanning time of 120 s (retrace time 15 s) and the average size
 114 distribution of 4 consecutive spectra was stored for further evaluation, resulting in a temporal
 115 resolution of 600 s (duty cycle 480 s). During 2014 the measuring period was from 1
 116 February through 30 April and from 12 August through 27 September. Due to technical
 117 problems we could not run the SMPS with the same configuration as in 2012, but used here a
 118 DMA model 3081 in combination with a CPC 3025A (TSI, $D_{p(50\%)}$ of 3 nm). Now, the air
 119 flow ratio was adjusted to enable size distribution measurements in the range between 6 nm
 120 and 213 nm. Note that due to the geometry of the DMA 3081, inherently longer particle
 121 residence time entailed perceptible particle losses resulting in enhanced uncertainties in the
 122 size distribution below 10 nm (according to the manufacturer, uncertainties in the size range
 123 between 10 nm and 6 nm could be about a factor of 1.5 to 2 higher for the DMA 3081
 124 compared to the DMA 3085). As in Dal Maso et al. (2005), we will use the terms nucleation
 125 mode for particles with $D_p < 25$ nm and Aitken mode for the size range $25 \text{ nm} \leq D_p < 100$ nm
 126 throughout the text.

127 Particle size distributions were evaluated along with continuous long-term condensation
 128 particle (CP) concentration measurements (CPC 3022A, TSI, $D_{p(50\%)}$ of 7 nm) and the ionic
 129 composition of the aerosol. For the latter, bulk aerosol sampling was regularly conducted in
 130 24-hour time periods using a teflon and a nylon filter in series (all 1 μm pore size). According
 131 to Piel et al. (2006) and Weller and Lampert (2008) samples were analyzed by ion
 132 chromatography for methane sulfonate (CH_3SO_3^- , MSA^-), Cl^- , Br^- , NO_3^- , SO_4^{2-} , Na^+ , NH_4^+ ,
 133 K^+ , Mg^{2+} , and Ca^{2+} . In addition aerosol light scattering measurements from a continuously
 134 operated three-wavelength integrating nephelometer (TSI, type 3563) were considered.
 135 Operation and data evaluation were explained in detail in Weller and Lampert 2008.
 136 Scattering Ångström exponents α were calculated according to

$$\alpha(\lambda_1 - \lambda_2) = \frac{\log(\sigma_{sp}(\lambda_1)/\sigma_{sp}(\lambda_2))}{\log(\lambda_1/\lambda_2)} \quad (1)$$

137 where $\alpha(\lambda_1-\lambda_2)$ refers to the wavelength pair λ_1 (nm) and λ_2 (nm) and $\sigma_{sp}(\lambda)$ are the total
138 scattering coefficients measured in Mm^{-1} ($1 \text{ Mm}^{-1} = 10^{-6} \text{ m}^{-1}$).

139 Meteorological data were available from the Meteorological Observatory at NM (a
140 description of the observatory itself and the installed meteorological sensors can be found
141 under: [http://www.awi.de/nc/en/science/long-term-observations/atmosphere/antarctic-
142 neumayer/meteorology.html](http://www.awi.de/nc/en/science/long-term-observations/atmosphere/antarctic-neumayer/meteorology.html), last access: 01 October 2015). The origin of the advected air
143 masses was assessed by 5-day backward trajectories provided by HYSPLIT 4.0 (Hybrid
144 Single-Particle Lagrangian Integrated trajectory;
145 http://www.arl.noaa.gov/documents/reports/hysplit_user_guide.pdf, last access: 01 October
146 2015). For all trajectory calculations we used GDAS meteorological data with a spatial
147 resolution of $1^\circ \times 1^\circ$ (longitude \times latitude grid). HYSPLIT trajectories also provide a crude
148 estimate of the vertical mixing height. Calculations were executed in one hour time steps. The
149 accuracy of the used 5-day back trajectories is difficult to assess (see e.g. review by Stohl,
150 1998). As outlined in Weller et al. (2014) above all the reliability of vertical wind components
151 could be problematic especially for regions like the Southern Ocean with sparse
152 meteorological input data (Harris et al., 2005). Thus we calculated all trajectories using the
153 3D wind fields of the GDAS data as well as employing the isentropic approximation. We
154 realized in some cases horizontal differences up to around 500 km between the starting points
155 of individual 5-day back trajectories calculated either under 3D or isentropic approximations,
156 but the general horizontal advection characteristic on which our conclusions were finally
157 based appeared robust. As to be expected, the vertical profile could significantly differ
158 between both approaches and should be regarded with particular caution. Finally, in order to
159 specify the characteristics of the local planetary boundary layer (PBL) we additionally gauged
160 vertical mixing in that layer as described in Weller et al. (2011a and 2014) by using the local
161 bulk Richardson number Ri_B (Stull, 1988).

162 **2.2 Data evaluation methods**

163 Particle concentrations, especially within the nucleation mode are susceptible to local
164 contamination. Hence data recorded under potential contamination conditions, indicated by

165 wind directions within a 330°-30° sector and/or wind velocities below 2.0 m s⁻¹ were
 166 removed. In addition black carbon (BC) concentrations were continuously monitored by a
 167 Multi Angle Absorption Photometer (MAAP model 5012, Thermo Electron Corp.), providing
 168 a supplemental criterion for local pollution when BC concentrations levels exceeded 100 ng
 169 m⁻³. Potential contamination happened only very sporadically within short periods (some
 170 hours at most) and on the whole, the actual data loss due to potential contamination was
 171 virtually negligible.

172 The crucial point of this study was to identify and characterize new particle formation. For
 173 this, we relied on the detailed criteria described by Dal Maso et al. (2005) and Kulmala et al.
 174 (2012). According to these recommendations, we defined a NPF event provided that particle
 175 size distribution starts within the nucleation mode ($D_p < 25$ nm) and prevailed for more than
 176 an hour. If the recorded size distribution spectra indicated particle growth, the linear growth
 177 rate (GR), defined as the change in particle diameter ΔD_p (nm) during a time step Δt (h) was
 178 determined by the so-called mode fitting method and in addition by the method of maximum
 179 concentration (Dal Maso et al., 2005; Yli-Juuti et al., 2011; Kulmala et al., 2012). We
 180 assumed that the GR was constant throughout the event and determined the GR by a linear fit
 181 through the geometric mean D_p (derived from the mode fitting procedure) at different times.
 182 In our case, nucleation mode and Aitken mode were generally well separated and log-normal
 183 distributions could be reliably fitted to the results. In contrast, the maximum concentration
 184 method resulted in somewhat higher GR compared to the mode fitting procedure (Table 1,
 185 values in parenthesis). However, the latter approach was occasionally not successful thus we
 186 relied on the mode fitting method. Finally we estimated nucleation particle formation rate for
 187 the size range between 3 nm and 25 nm defined by:

$$J_{3-25} = \frac{UCP_{3-25}}{\Delta t} \quad (2)$$

188 Here, UCP_{3-25} (ultrafine condensation particles) is the particle concentration in the size range
 189 between 3 nm and 25 nm derived from the SMPS data. Note that our approach to calculate
 190 particle formation as well as GR presumes a homogenous air mass and thus neglects the
 191 impact of changing air mass advection. Unfortunately, particle size distribution data were

192 only available from 3 nm to 64 nm and 6 nm to 213 nm, respectively, hence an appropriate
 193 calculation of coagulation and condensation losses to correct GR and particle formation rate
 194 was impossible, but should usually be negligible in clean, homogeneous air masses (Kulmala
 195 et al., 2004a; Leppä et al., 2011). In fact, during both campaigns, total CP concentrations
 196 measured by the CPC 3022A were typically below 1000 cm^{-3} and only very rarely reached
 197 2000 cm^{-3} . In addition, during all NPF events nucleation mode particles ($D_p < 25 \text{ nm}$)
 198 constituted the major component of the total CP concentration. According to Leppä et al.
 199 (2011), self-coagulation and coagulation scavenging might have distorted in our case growth
 200 rates well below 0.03 nm h^{-1} and 0.02 nm h^{-1} , respectively, corresponding to a condensation
 201 sink (CS) $< 2 \times 10^{-3} \text{ s}^{-1}$. Virkkula et al. (2011) estimated CS using light scattering data from
 202 nephelometer measurements. Adapting the calibration presented therein and the actually
 203 observed $\sigma_{\text{sp}}(550)$ values during NPF events at NM (typically below 5 Mm^{-1}) indicated again
 204 a CS around 10^{-3} s^{-1} .

205 According to Nieminen et al. (2010) and Yli-Juuti et al. (2011), we finally estimated the
 206 H_2SO_4 vapour concentration needed for the calculated GR, assuming that H_2SO_4 was the sole
 207 component responsible for the observed particle growth (kinetic regime, $D_p \ll 60 \text{ nm}$):

$$GR = \frac{\gamma \cdot m_v \cdot v_{\text{mol}}}{4\rho} \cdot c_{\text{vapour}} \quad (3)$$

208 with m_v = molecular mass of the vapour (98 g mole^{-1}), ρ = density of the condensed vapour
 209 (1.6 g cm^{-3} assuming a $\text{H}_2\text{SO}_4/\text{H}_2\text{O}$ mixture of 68% H_2SO_4 by weight at 273 K), v_{mol} = gas
 210 kinetic velocity of the vapour molecules (e.g. 242 m s^{-1} for $T = 273 \text{ K}$), c_{vapour} = gaseous
 211 H_2SO_4 concentration (mole cm^{-3}) to be determined, and γ is close to the H_2SO_4
 212 accommodation coefficient (assumed to be around 1.0).

213

214 **3 Results**215 **3.1 Data presentation**

216 During the first summer campaign in 2012 (comprising 66 observation days and 9500 raw
217 spectra) we identified 19 events of NPF without clearly discernible particle growth (class II
218 events according to Dal Maso et al., 2005). Growth rates could be reliably determined in 8
219 class I or so-called "banana-type" events (Dal Maso et al., 2005). An overview of size
220 resolved aerosol data for the months January through March 2012 as well as a selected series
221 of consecutive NPF events is presented in the Supplementary Material (Figs. S.1 and S.2)
222 together with concurrently measured total CP concentrations, meteorological parameters, and
223 the ionic composition of the bulk aerosol (SMPS data from both campaigns reported here are
224 available at <http://dx.doi.org/10.1594/PANGAEA.845024> and auxiliary data can be found in
225 the Supplementary Material). Figure 1 focuses on a striking NPF event happened on January
226 27, where a simultaneous nucleation- and Aitken mode growth was evident. This NPF event
227 will be further discussed as case study in 4.1. Figure 2 shows a more detailed topographic
228 view of this event on a linear $dN/d\log D_p$ scale and is supplemented by corresponding profiles
229 of log-normal distribution fits from selected time slices. In addition, a strikingly prolonged
230 Aitken mode growth over about 3 days ($GR = 0.3 \pm 0.05 \text{ nm h}^{-1}$) started at 1 March (doy 61)
231 but without exhibiting a discernible nucleation mode (Supplementary Material, Fig. S.2).
232 Particle concentrations in the nucleation mode were strongly correlated with total CP
233 concentrations measured by the CPC 3022A (Supplementary Material, Fig. S.1b). A
234 correlation of particle concentrations measured by the SMPS in the range between 5 nm and
235 64 nm with CP concentrations revealed a linear dependence (slope 0.992, $r^2 = 0.8$; see Fig.
236 S.3 in the Supplementary Material), indicating that during summer CP number concentrations
237 were dominated by nucleation and Aitken mode particles.

238 In contrast, the yield of NPF events during summer 2014 (February through April 2014, 85
239 observation days, 12240 raw spectra) was rather scanty: Apart from 15 class II events, only 2

240 class I events could be discerned. A presentation of this time series can again be found in the
241 Supplementary Material (Fig. S.4). During winter (August and September 2014, 37.5
242 observation days, 5370 raw spectra), two certain class II events were evident (14/15 August
243 and 21 September, Fig. 3). Figure 4 presents the mean particle size distribution during both
244 winter events and for comparison for a typical non-event day (18 August 2014). Table 1
245 summarizes all evaluated class I events and lists the calculated GR, nucleation particle
246 formation rates (J_{3-25}) and the estimated H_2SO_4 concentration hypothetically needed for the
247 respective GR.

248 **3.2 Meteorological aspects**

249 Regarding local meteorology, virtually all NPF events observed at NM occurred during
250 southerly wind directions ($180^\circ \pm 60^\circ$) with wind velocities below 12 m s^{-1} (typically between
251 4 m s^{-1} and 8 m s^{-1}). Usually bright weather conditions prevailed with a cloud amount below 3
252 Octans and a relative sun shine duration around $(48 \pm 26)\%$ relating to clear sky conditions,
253 except for three NPF events occurring during cloud covered sky (25 February 2012, 08 and 09
254 March 2012). In all cases the local PBL was characterized by Ri_B numbers < 0.25 , indicating
255 turbulent flow and a well-mixed PBL. This was supported by HYSPLIT back trajectory
256 analyses indicating vertical mixing heights around 250 m (range: 100 m to 600 m) for the last
257 6 hours before arrival at NM (5-day back trajectories for the most prominent nucleation
258 events are presented in the Supplementary Material, Fig. S.5). Note, however that mixing
259 heights provided by HYSPLIT should be treated as a rough estimate, particularly regarding
260 the Antarctica PBL due to the impact of katabatic winds and uncertain vertical wind
261 components in general. The spatial extend of NPF events associated with appreciable particle
262 growth could be estimated to be around $170 \pm 85 \text{ km}$, taking into account the prevailing wind
263 velocity (around $8 \pm 4 \text{ m s}^{-1}$) and the confined NPF duration (around 6 hours, Table 1).
264 Backward trajectories for NPF events revealed that frequently air masses originated from the
265 marine boundary layer (MBL) of the South Atlantic and then typically travelled along the
266 Antarctic coastline up to five days before arrival at NM (Supplementary Material Fig. S.5). A
267 subsequent contact time of these trajectories with open water or sea ice was rather limited and

268 often happened, if at all, just some hours before arrival at NM. During NPF events trajectories
269 mainly stayed below 1500 m above ground for the last 48 hours before arrival at NM and
270 mainly within the vertical mixing heights derived from HYSPLIT for the last 24 hours. Only
271 for the NPF event at 16 March 2012 air masses clearly descended from the free troposphere
272 (in this case >2000 m above ground) within the last 24 hours before arrival at NM. In
273 summary, NPF related trajectories indicate the importance of recent MBL air advection while
274 the impact of descending air masses from the free troposphere seems to be rare. On the whole
275 trajectory analyses appeared somewhat equivocal in evaluating a rather local process like
276 NPF, probably because of their particularly inherent spatial uncertainty in a region sparsely
277 supported by meteorological data.

278 During summer, nucleation events showed a distinct diurnal cycle. They typically occurred in
279 the second half of the day indicating a link to local photochemistry, though being sometimes
280 delayed to the diurnal maximum of UV radiation by a few hours (Figs. 1 and S.2; Table 1).
281 We did not discover a meaningful relation between UV irradiance and GR or particle
282 formation rate. Table 2 presents a comparison of selected auxiliary parameters during NPF
283 and non-event days. In summary, NPF events tend to be accompanied by drier air (impact of
284 southerly, continental advection), lower aerosol light scattering coefficients (indicating lower
285 particle surface area), and less aerosol mass. Winter events happened either several hours
286 around midnight or more than day-long (Fig. 3) and the measured maximum UV radiance was
287 4 W m^{-2} and 18 W m^{-2} for the NPF event observed on August and September, respectively.
288 Again, respecting 5-day back trajectories documented a similar advection pattern as for the
289 summertime NPF events (Supplementary Material Fig. S.6).

290 During stormy weather, occasionally enhanced particle concentrations appeared below 10 nm.
291 In this context, it is worth to mention that Virkkula et al. (2007) and Asmi et al. (2010)
292 observed at Aboa some nucleation events associated with high wind speeds and suggested ion
293 production by fast moving ice crystals followed by subsequent ion-mediated nucleation. As
294 for NM the situation was somewhat unclear, because charged particle concentration data were
295 not available and during stormy weather the overall electrostatic charge in combination with

296 inherently critical electrical grounding conditions on ice may have provoked instrumental
297 artefacts.

298

299 **4 Discussion**

300 **4.1 Case study**

301 A striking series of NPF occurred during three days, starting around noon at 26 January 2012
302 with a class II event (Fig. 1a), accompanied by an immediate increase of UCP₃₋₂₅
303 concentration (Fig. 1b). Around noon two size distribution maxima were discernible below 25
304 nm, one around 6 nm, the other between 15 nm and 20 nm. While the first one disappeared
305 after 16:00 UTC, the latter lingered on and started to grow between 07:00 and 14:00 UTC
306 next day ($GR = 1.9 \text{ nm h}^{-1}$, Table 1), finally reaching a mode maximum around 50 nm after a
307 further growth during the afternoon of 28 January 2012. Coinciding with particle growth, the
308 difference between CP and UCP₃₋₂₅ concentrations steeply increased due to particle formation
309 in the size range $D_p > 25 \text{ nm}$. Starting at 11:00 UTC on 27 January 2012 a class I NPF event
310 was observed showing particle growth from around 7 nm to 20 nm during the following 7
311 hours. Particle growth started again during the afternoon of 28 January 2012 eventually
312 reaching a mode maximum around 25 nm (Fig. 1a and Fig. 2).

313 Interestingly, this class I NPF event commenced immediately after a striking peak in light
314 scattering coefficients (Fig. 1d). Given that nephelometer measurements are primarily
315 sensitive to particle concentrations within a size range comparable to the measuring
316 wavelengths, this peak indicated simultaneously enhanced accumulation mode particle
317 concentrations. One may argue that enhanced accumulation mode particles acted as additional
318 CS and inhibited NPF, but this would be inconsistent to the observed distinct growth of the 15
319 nm nucleation mode from the previous day already starting at 07:00 UTC. Concerning
320 meteorological and radiation conditions, all three days were virtually cloudless (as can also be
321 deduced from the smooth and nearly sinusoidal $UV_{300-370}$ signal, Fig. 1d) and southerly
322 advection dominated. Trajectory analyses revealed that air masses had actually no contact

323 with the MBL for at least 48 hours before, but most of them originated in the MBL of the
324 South Atlantic (Fig. 5) about 5 days before. This finding suggested a long range transport of
325 marine precursor gases associated with a delayed nucleation just before arrival at NM. Except
326 a short period around 02:00 UTC at 28/01/2012, Ri_B values indicated a well-mixed boundary
327 layer (Fig. 1c).

328 From the measured size distribution spectra we calculated the total aerosol mass concentration
329 m_p between 3 nm and 64 nm, assuming a particle density of 1.8 g cm^{-3} (according to pure
330 H_2SO_4 as an upper limit for dry sulfuric acid aerosol). The result is presented in Fig. 1e
331 together with the ionic composition of the aerosol derived from our daily aerosol sampling.
332 MSA^- and nss-SO_4^{2-} mass concentrations increased throughout, while those of Na^+ (a tracer
333 for sea salt aerosol) and NH_4^+ remained low (note that the time of the filter exchange is
334 marked with vertical red lines). The stepwise increase of m_p appeared roughly comparable to
335 the increase of nss-SO_4^{2-} mass concentrations from day to day. Note, that this estimate
336 presumes pure sulfuric acid aerosol and should thus be treated as upper limit assessment.
337 Furthermore, based on our measurements we cannot finally deduce whether H_2SO_4 vapour
338 genuinely condensed on freshly formed nucleation mode particles or merely on aged
339 background aerosol.

340 **4.2 Extent of particle growth**

341 In view of previous results from Antarctica (Asmi et al., 2010, Järvinen et al., 2013; Kyrö et
342 al., 2013), NPF at NM appeared notably less efficient. Particle growth was usually confined to
343 the nucleation mode and only once extended into the Aitken mode (see case study described
344 in 4.1). Consequently, this NPF event was the only one at NM where the growth of nucleated
345 particles reached a size range potentially relevant for acting as CCN. On the other hand, a
346 persistent, but not locally developed Aitken mode was often present during polar day
347 (Supplementary Material S.1) and after being missing in August reappeared in September
348 (Fig. 3). Notwithstanding, some discrete events with strikingly high particle concentrations
349 between 30 nm and 200 nm occurred in August exclusively under stormy weather (wind
350 velocity around 20 m s^{-1} ; Fig. 3). Contemporaneously, Na^+ concentrations increased from

351 back-ground levels around 80 ng m^{-3} to values between 480 ng m^{-3} and 1010 ng m^{-3} .
352 According to impactor measurements conducted by Teinilä et al. (2014) in the year 2010 at
353 NM, most probably sub- μm sea salt aerosol might also have caused the latter peculiarities.

354 **4.3 Role of DMS derived sulfuric acid and MSA**

355 Although air mass advection pattern assessed by trajectory calculations turned out to be
356 equivocal, the observed diurnal cycle of NPF and the ionic composition of the aerosol
357 indicate that particle nucleation at NM was most probably induced by emissions of marine
358 biogenic precursor gases (Yu and Luo, 2010). More precisely, photo-oxidation of
359 phytoplankton derived dimethyl sulfide (DMS) is in general the prominent photochemical
360 process in the troposphere of coastal Antarctica (e.g. Minikin et al., 1998), yielding ultimately
361 sulfuric acid (H_2SO_4) and methane sulfonic acid (MSA, $\text{CH}_3\text{SO}_3\text{H}$). Nevertheless, and in
362 agreement with results from other Antarctic sites (Järvinen et al., 2013; Kyrö et al., 2013),
363 H_2SO_4 concentrations needed for the observed growth rates should be at least an order of
364 magnitude higher compared to available values actually observed in Antarctica: Jefferson et
365 al. (1998) measured mean H_2SO_4 concentrations around $1.6 \times 10^6 \text{ molec cm}^{-3}$ during the
366 SCATE campaign at Palmer Station (Antarctic Peninsula) in summer, and at South Pole
367 during the ISCAT 2000 campaign H_2SO_4 (MSA) concentrations around $0.27 \times 10^6 \text{ molec cm}^{-3}$
368 ($0.08 \times 10^6 \text{ molec cm}^{-3}$) were detected in December (Mauldin III et al., 2004). Although the
369 chemical composition of secondary aerosol during summer at NM was usually dominated by
370 DMS derived nss-SO_4^{2-} and MS (Weller and Lampert 2008; Weller et al., 2011b), according
371 to this estimate observed particle growth in the early stage should yet be controlled by other
372 low volatile vapours.

373 **4.4 Possible role of H_2O vapour, NH_3 , organic vapour, iodine oxide, and ions**

374 Theoretical and laboratory studies revealed that H_2O molecules are important for early
375 particle growth (2-3 nm) due to stabilization of the critical nucleus by H_2SO_4 -hydrate
376 formation, while further particle growth is dominated by H_2SO_4 or low volatile organic
377 vapours (Nieminen et al., 2010; Zhang et al., 2012). These investigations indicated that under

378 prevalent atmospheric conditions nucleation rate might be correlated with relative humidity
379 (rH), depending on NH₃ and organic vapour concentrations (Zhang et al., 2012). Concerning
380 this point, our data were inconclusive: It seems, though in contrast to the above mentioned
381 investigations, that NPF events sometimes occurred during rH decrease (Supplementary
382 Material, Fig. S.2). But this apparent correlation was particularly due to the fact that we
383 mainly observed NPF in the afternoon when increasing temperatures usually induced
384 decreasing rH levels. In addition, a correlation between H₂O vapour partial pressure (i.e.
385 absolute humidity) and nucleation rates derived from equation (1) was absent.

386 Apart from H₂SO₄ and H₂O vapour, gaseous precursors like NH₃, organic vapours (notably
387 organic amines), and inorganic iodine compounds (mainly iodine oxides) are known to be
388 strongly involved in particle nucleation and particle growth (O'Dowd et al., 2002b; Kulmala
389 et al., 2004b; Facchini et al., 2008a; McFiggans et al., 2010; Metzger et al., 2010; Benson et
390 al., 2011; Dawson et al., 2012; Riccobono et al., 2012; Riipinen et al., 2012; Wang et al.,
391 2013). As for NH₃, previous thermodenuder measurements at NM indicated that biogenic
392 secondary aerosol was likely an internal mixture of the acids H₂SO₄ and MSA partly
393 neutralized by NH₃ (Weller et al., 2011a). Actually, we observed NH₄⁺ concentrations at NM
394 of around 10 ng m⁻³. Preliminary results on the amount of water soluble organic carbon
395 (WSOC, excluding MSA), determined from bulk filter samples taken during austral summer
396 2011 showed values between 5 and 35 ngC m⁻³ (method: solid phase extraction followed by
397 TOC analysis; Lehmann, personal communication 2015). Interestingly, NH₄⁺ and WSOC
398 concentrations appeared thus similar to values reported from Aboa (Asmi et al., 2010) where
399 particle growth was more pronounced. At Aboa, biogenic emissions by nearby melting ponds
400 were found to be a potential source for condensable vapour (Kyrö et al., 2013), while the
401 surroundings of NM are completely ice covered throughout (apart from open water dependent
402 on seasonal sea ice coverage) and the nearest insular rocky outcrops are more than 200 km
403 away. One may speculate that marine primary organic aerosol was dominant at NM, linked
404 with sea spray formation by bubble bursting (Facchini et al., 2008b), while at Aboa
405 condensable organic vapour emissions from melting ponds were decisive.

406 From the mid-latitude European sites Roscoff and Mace Head there exists strong evidence for
407 iodine mediated NPF (O'Dowd et al., 2002b; McFiggans et al., 2010) and in recent studies, a
408 possible impact of IO on NPF in the Arctic (Allan et al., 2014) and particle number
409 concentrations at Halley Station, Antarctica (Roscoe et al., 2015) were inferred. Concerning
410 iodine compounds, in situ measurements by long-path Differential Optical Absorption
411 Spectroscopy (LP-DOAS) conducted at Halley (Saiz-Lopez et al., 2007) as well as respective
412 satellite observations (Schönhardt et al., 2012) revealed maximum IO concentration of some 5
413 pptv (volume parts per trillion) over Antarctic coastal regions around October. Such IO levels
414 were comparable to coastal European sites like Roscoff and Mace Head (O'Dowd et al.,
415 2002b; McFiggans et al., 2010). At NM, multi-axis (MAX) DOAS measurements using
416 scattered skylight primarily provided IO column densities, which did not show a discernible
417 seasonality (Frieß et al., 2010). Note that MAX-DOAS measurements were only available
418 during clear sky conditions and solar zenith angles $< 85^\circ$ and were not available regarding the
419 observed winter NPF events. Presuming that IO was restricted within the PBL (below 2 km),
420 comparable IO mixing ratios in the range of some pptv could be derived for NM in some
421 cases, but this approach is actually highly uncertain (Frieß et al., 2001 and 2010).
422 Interestingly, at Dumont d'Urville (DDU), IO concentrations were found to be an order of
423 magnitude lower indicating that halogen chemistry in general was probably promoted by the
424 much larger sea ice extend of the Atlantic sector of Antarctica (Grilli et al., 2013).
425 Considering the available laboratory-, field- and model results, it appears difficult to estimate
426 IO concentrations needed to provoke significant particle nucleation but it seems that several
427 pptv IO or OIO would be necessary (Pechtl et al., 2006; Saiz-Lopez et al., 2012; Roscoe et al.,
428 2015). In view of the minor importance of DMS photochemistry, however, we speculate that
429 IO probably initiated the observed NPF at NM in late winter. The shape of both winter events
430 and the fact that growth rates could not be determined indicated a local origin where particle
431 size distribution developed during transport time to the measuring site (Kulmala et al., 2012).

432 At last, given that in our case particle formation rates J_{3-25} were generally below $0.1 \text{ cm}^{-3} \text{ s}^{-1}$,
433 atmospheric ions could have significantly contributed to particle nucleation at NM (Almeida
434 et al., 2013, Fig. 2 therein). In this regard, a modelling study by Yu and Luo (2010)

435 demonstrated that NPF in coastal Antarctic regions can be reasonably described by ion
436 mediated $\text{H}_2\text{SO}_4/\text{H}_2\text{O}$ nucleation.

437

438 **5 Conclusions**

439 Based on our data we can only speculate about the prevailing nucleation mechanism at NM,
440 but our findings are essentially consistent with $\text{H}_2\text{SO}_4/\text{NH}_3/\text{H}_2\text{O}$ ternary and/or $\text{H}_2\text{SO}_4/\text{H}_2\text{O}$
441 ion mediated nucleation during summer. In contrast, the observed particle growth was
442 governed by the availability of other yet not identified gaseous precursors, most probably low
443 volatile organic compounds of marine origin. Due to the apparent deficit of the latter, particle
444 growth was accordingly restricted within the nucleation mode and in the main did not extend
445 to particle diameter ranges relevant for acting as cloud condensation nuclei. Given that
446 particle growth in the early stage (i.e. within the nucleation mode) was governed by low
447 volatile vapours other than H_2SO_4 , another remaining crucial question is, in which way the
448 finally sulfuric acid dominated secondary aerosol at NM was ultimately generated. During
449 summer, a potential role of iodine oxides in particle nucleation was unclear, while for the
450 observed winter events these compounds could be potential candidates. But then, the even
451 more pronounced deficit of condensable vapour due to depressed photochemical activity
452 impeded particle growth beyond particle diameters of about 15 nm.

453 In conclusion, our investigations indicate three crucial points concerning NPF in Antarctica
454 that are supposed to be addressed in future work: (i) Up to now, from this region only sparse
455 and inadequate knowledge exists on organic aerosols, in particular secondary organic aerosol.
456 Identification of the most important compounds, their origin and source strength is still
457 fragmentary at best. (ii) IO concentrations should be measured year-round by in-situ
458 techniques in order to better assess its role in NPF and validate respecting satellite retrievals.
459 (iii) The role of free tropospheric air in providing gaseous precursor for particle nucleation
460 and growth within the PBL needs clarification. This point appeared especially important for
461 continental Antarctica in view of the recently described NPF events observed at Dome C
462 (Järvinen et al., 2013).

463

464 **Acknowledgements**

465 The authors would like to thank the technicians and scientists of the Neumayer overwintering
466 teams of the years 2012 and 2013, whose outstanding commitment enabled continuous high
467 quality measurements. RH and KT thank Academy of Finland for the financial support
468 (project ACPANT, decision nr 264375). Special thanks go to Kathrin Höppner, responsible
469 for the Air Chemistry Observatory during the overwintering 2012, to Udo Frieß for beneficial
470 discussions respecting IO concentrations at NM, and finally to Astrid Lampert for many
471 fruitful suggestions. We are thankful to NOAA Air Resources Laboratory for having made
472 available the HYSPLIT trajectory calculation program as well as all used input data files.

473

474 **References**

- 475 Allan, J. D., Williams, P. I., Najera, J., Whitehead, J. D., Flynn, M. J., Taylor, J. W., Liu, D.,
476 Darbyshire, E., Carpenter, L. J., Chance, R., Andrews, S. J., Hackenberg, S. C., and
477 McFiggans, G.: Iodine observed in new particle formation events in the Arctic atmosphere
478 during ACCACIA, *Atmos. Chem. Phys.*, 15, 5599-5609, doi:10.5194/acp-15-5599-2015,
479 2015.
- 480 Almeida, J., Schobesberger, S., Kürten, A., Ortega, I. K., Kupiainen-Määttä, O., Praplan, A.
481 P., Adamov, A., Amorim, A., Bianchi, F., Breitenlechner, M., David, A., Dommen, J.,
482 Donahue, N. M., Downard, A., Dunne, E. M., Duplissy, J., Ehrhart, S., Flagan, R. C.,
483 Franchin, A., Guida, R., Hakala, J., Hansel, A., Heinritzi, M., Henschel, H., Jokinen, T.,
484 Junninen, H., Kajos, M., Kangasluoma, J., Keskinen, H., Kupc, A., Kurtén, T., Kvashin, A.
485 N., Laaksonen, A., Lehtipalo, K., Leiminger, M., Leppä, J., Loukonen, V., Makhmutov, V.,
486 Mathot, S., McGrath, M. J., Nieminen, T., Olenius, T., Onnela, A., Petäjä, T., Riccobono, F.,
487 Riipinen, I., Rissanen, M., Rondo, L., Ruuskanen, T., Santos, F. D., Sarnela, N., Schallhart,
488 S., Schnitzhofer, R., Seinfeld, J. H., Simon, M., Sipilä, M., Stozhkov, Y., Stratmann, F.,
489 Tomé, A., Tröstl, J., Tsagkogeorgas, G., Vaattovaara, P., Viisanen, Y., Virtanen, A., Vrtala,
490 A., Wagner, P. E., Weingartner, E., Wex, H., Williamson, C., Wimmer, D., Ye, P., Yli-Juuti,
491 T., Carslaw, K. S., Kulmala, M., Curtius, J., Baltensperger, U., Worsnop, D. R., Vehkamäki,
492 H., and Kirkby, J.: Molecular understanding of sulphuric acid-amine particle nucleation in the
493 atmosphere, *Nature*, 502, 359–363, 2013.
- 494 Asmi, E., Frey, A., Virkkula, A., Ehn, M., Manninen, H.E., Timonen, H., Tolonen-Kivimäki,
495 O., Aurela, M., Hillamo, R., and Kulmala, M.: Hygroscopicity and chemical composition of
496 Antarctic sub-micrometer aerosol particles and observations of new particle formation,
497 *Atmos. Chem. Phys.*, 10, 4253-4271, doi:10.5194/acp-10-4253-2010, 2010.
- 498 Benson, D. R., Yu, J. H., Markovich, A., and Lee, S.-H.: Ternary homogeneous nucleation of
499 H₂SO₄, NH₃, and H₂O under conditions relevant to the lower troposphere, *Atmos. Chem.*
500 *Phys.*, 11, 4755-4766, doi:10.5194/acp-11-4755-2011, 2011.

- 501 Boucher, O., Randall, D., Artaxo, P., Bretherton, C., Feingold, G., Forster, P., Kerminen, V.-
502 M., Kondo, Y., Liao, H., Lohmann, U., Rasch, P., Satheesh, S.K., Sherwood, S., Stevens B.,
503 and Zhang, X.Y.: Clouds and Aerosols. In: *Climate Change 2013: The Physical Science*
504 *Basis. Contribution of Working Group I to the Fifth Assessment Report of the*
505 *Intergovernmental Panel on Climate Change* [Stocker, T.F., Qin, D., Plattner, G.-K., Tignor,
506 M., Allen, S.K., Boschung, J., Nauels, A., Xia, Y., Bex V., and Midgley P.M. (eds.)].
507 Cambridge University Press, Cambridge, United Kingdom and New York, NY, USA, 2013.
- 508 Bzdek, B. and Johnston, M.V.: New Particle Formation and Growth in the Troposphere, *Anal.*
509 *Chem.*, 82, No. 19, 7871-7878, doi:10.1021/ac100856j, 2010.
- 510 Carslaw, K.S., Lee, L.A., Reddington, C.L., Pringle, K.J., Rap, A., Forster, P.M., Mann,
511 G.W., Spracklen, D.V., Woodhouse, M.T., Regayre, L.A. and Pierce, J.R.: Large contribution
512 of natural aerosol to uncertainty in indirect forcing, *Nature*, 503, 67-71,
513 doi:10.1038/nature12674, 2013.
- 514 Dal Maso, M., Kulmala, M., Riipinen, I., Wagner, R., Hussein, T., Aalto, P.P., and Lehtinen,
515 E.J.: Formation and growth of fresh atmospheric aerosols: eight years of aerosol size
516 distribution data from SMEAR II, Hyytiälä, Finland, *Boreal Env. Res.*, 10, 323-336, 2005.
- 517 Dawson, M.L., Varner, M.E., Perraud, V., Ezell, M.J., Gerber, R.B., and Finlayson-Pitts, B.J.:
518 Simplified mechanism for new particle formation from methanesulfonic acid, amines, and
519 water via experiments and ab initio calculations, *PNAS*, 109 (46), 18719-18724,
520 doi:10.1073/pnas.1211878109, 2012.
- 521 Facchini, M.C., Decesari, S., Rinaldi, M., Carbone, C., Finessi, E., Mircea, M., Fuzzi, S.,
522 Moretti, F., Tagliavini, E., Ceburnis, D., and O'Dowd, C.D.: Important Source of Marine
523 Secondary Organic Aerosol from Biogenic Amines, *Environ. Sci. Technol.*, 42 (24), 9116-
524 9121, 2008a.
- 525 Facchini, M.C., Rinaldi, M., Decesari, S., Carbone, C., Finessi, E., Mircea, M., Fuzzi, S.,
526 Ceburnis, D., Flanagan, R., Nilsson, E.D., de Leeuw, G., Martino, M., Woeltjen, J., and
527 O'Dowd, C.D.: Primary submicron marine aerosol dominated by insoluble organic colloids
528 and aggregates, *Geophys. Res. Lett.*, 35, L17814, doi:10.1029/2008GL034210, 2008b.

- 529 Frieß, U., Wagner, T., Pundt, I., Pfeilsticker, K., and Platt, U.: Spectroscopic Measurements
530 of Tropospheric Iodine Oxide at Neumayer Station, Antarctica, *Geophys. Res. Lett.*, 28, 1941-
531 1944, doi:10.1029/2000GL012784, 2001.
- 532 Frieß, U., Deutschmann, T., Gilfedder, B. S., Weller, R., and Platt, U.: Iodine monoxide in the
533 Antarctic snowpack, *Atmos. Chem. Phys.*, 10, 2439-2456, doi:10.5194/acp-10-2439-2010,
534 2010.
- 535 Grilli, R., Legrand, M., Kukui, A., Méjean, G., Preunkert, S., and Romanini, D.: First
536 investigations of IO, BrO, and NO₂ summer atmospheric levels at a coastal East Antarctic site
537 using mode-locked cavity enhanced absorption spectroscopy, *Geophys. Res. Lett.*, 40, 791-
538 796, doi:10.1002/grl.50154, 2013.
- 539 Harris, J.M., Draxler, R.R., and Oltmans, S.J.: Trajectory model sensitivity to differences in
540 input data and vertical transport method, *J. Geophys. Res.*, 110, D14109,
541 doi:10.1029/2004JD005750, 2005.
- 542 Haywood, J. and Boucher, O.: Estimates of the direct and indirect radiative forcing due to
543 tropospheric aerosols: A review, *Rev. Geophys.*, 38(4), 513-543, 2000.
- 544 Henze, D.K. and Seinfeld, J.H.: Global secondary organic aerosol from isoprene oxidation,
545 *Geophys. Res. Lett.*, 33, L09812, doi:10.1029/2006GL025976, 2006.
- 546 Humphries, R. S., Schofield, R., Keywood, M., Ward, J., Pierce, J. R., Gionfriddo, C. M.,
547 Tate, M., Krabbenhoft, D., Galbally, I. E., Molloy, S. B., Klekociuk, A., Johnston, P. V.,
548 Kreher, K., Thomas, A. J., Robinson, A. D., Harris, N. R. P., Johnson, R., and Wilson, S. R.:
549 Boundary layer new particle formation over East Antarctic sea ice – possible Hg driven
550 nucleation?, *Atmos. Chem. Phys. Discuss.*, 15, 19477-19536, doi:10.5194/acpd-15-19477-
551 2015, 2015.
- 552 Ito, T.: Study of background aerosols in the Antarctic Troposphere, *J. Atmos. Chem.* 3, 69-91,
553 1985.
- 554 Ito, T.: Size distribution of Antarctic submicron aerosols, *Tellus*, 45B, 145-159, 1993.

- 555 Jaenicke, R., Dreiling, V., Lehmann, E., Koutsenogui, P.K., and Stingl, J.: Condensation
556 nuclei at the German Antarctic Station „Georg von Neumayer“, *Tellus*, 44B, 311-317, 1992.
- 557 Järvinen, E., Virkkula, A., Nieminen, T., Aalto, P. P., Asmi, E., Lanconelli, C., Busetto, M.,
558 Lupi, A., Schioppo, R., Vitale, V., Mazzola, M., Petäjä, T., Kerminen, V.-M., and Kulmala,
559 M.: Seasonal cycle and modal structure of particle number size distribution at Dome C,
560 Antarctica, *Atmos. Chem. Phys.*, 13, 7473-7487, doi:10.5194/acp-13-7473-2013, 2013.
- 561 Jefferson, A., Tanner, D.J., Eisele, F.L., Davis, D.D., Chen, G., Crawford, J., Huey, J.W.,
562 Torres, A.L., and Berresheim, H: OH photochemistry and methane sulfonic acid formation in
563 the coastal Antarctic boundary layer, *J. Geophys. Res.*, 103(D1), 1647-1656, 1998.
- 564 König-Langlo, G., King, J.C., Pettré, P.: Climatology of the three coastal Antarctic stations
565 Dumont d'Urville, Neumayer and Halley, *J. Geophys. Res.*, 103(D9), 10,935-10,946, 1998.
- 566 Koponen, I.K., Virkkula, A., Hillamo, R., Kerminen, V.-M., Kulmala, M.: Number size
567 distribution and concentrations of the continental summer aerosol in Queen Maud Land,
568 Antarctica, *J. Geophys. Res.*, 108(D18), 4587, doi:10.1029/2003JD003614, 2003.
- 569 Korhonen, H., Carslaw, K.S., Spracklen, D.V., Mann, G.W., and Woodhouse, M.T.: Influence
570 of oceanic dimethyl sulfide emissions on cloud condensation nuclei concentrations and
571 seasonality over the remote Southern Hemisphere oceans: A global model study, *J. Geophys.*
572 *Res.*, 113(D15204), doi:10.1029/2007JD009718, 2008.
- 573 Kulmala, M., Vehkamäki, H., Petäjä, T., Dal Maso, M., Lauri, A., Kerminen, V.-M., Birmili,
574 W., McMurry, P.H.: Formation and growth rates of ultrafine atmospheric particles: a review
575 of observations, *Aerosol Sci.*, 35, 143-176, doi:10.1016/j.jaerosci.2003.10.003, 2004a.
- 576 Kulmala, M., Kerminen, V.-M., Anttila, T., Laaksonen, A., and O'Dowd, D: Organic aerosol
577 formation via sulphate cluster activation, *J. Geophys. Res.*, 109 (D04205,
578 doi:10.1029/2003JD003961, 2004b.
- 579 Kulmala, M., Petäjä, T., Nieminen, T., Sipilä, M., Manninen, H.E., Lehtipalo, K., Dal Maso,
580 M., Aalto, P.P., Junninen, H., Paasonen, P., Riipinen, I., Lehtinen, K.E.J., Laaksonen, A., and

- 581 Kerminen, V.-M.: Measurements of the nucleation of atmospheric aerosol particles. *Nature*
582 *Protocols*, Vol.7 No.9, 1651-1667, doi:10.1038/nprot.2012.091, 2012.
- 583 Kyrö, E.-M., Kerminen, V.-M., Virkkula, A., Dal Maso, M., Parshintsev, J., Ruíz-Jimenez, J.,
584 Forsström, L., Manninen, H. E., Riekkola, M.-L., Heinonen, P., and Kulmala, M.: Antarctic
585 new particle formation from continental biogenic precursors, *Atmos. Chem. Phys.*, 13, 3527-
586 3546, doi:10.5194/acp-13-3527-2013, 2013.
- 587 Leppä, J., Anttila, T., Kerminen, V.-M., Kulmala, M., and Lehtinen, K. E. J.: Atmospheric
588 new particle formation: real and apparent growth of neutral and charged particles, *Atmos.*
589 *Chem. Phys.*, 11, 4939-4955, doi:10.5194/acp-11-4939-2011, 2011.
- 590 Mauldin III, R.L., Kosciuch, E., Henry, B., Eisele, F.L., Shetter, R., Lefer, B., Chen, G.,
591 Davis, D., Huey, G., Tanner, D.: Measurements of OH, HO₂+RO₂, H₂SO₄, and MSA at the
592 South Pole during ISCAT 2000, *Atmos. Environ.*, 38, 5423-5437, 2004.
- 593 McFiggans, G., Bale, C.S.E., Ball, S.M., Beames, J.M., Bloss, W.J., Carpenter, L.J., Dorsey,
594 J., Dunk, Flynn, M.J., Furneaux, K.L., Gallagher, M.W., Heard, D.E., Hollingsworth, A.M.,
595 Hornsby, K., Ingham, T., Jones, C.E., Jones, R.L., Kramer, L.J., Langridge, J.M., Leblanc, C.,
596 LeCrane, J.-P., Lee, J.D., Leigh, R.J., Longley, I., Mahajan, A.S., Monks, P.S., Oetjen, H.,
597 Orr-Ewing, A.J., Plane, J.M.C., Potin, P., Shillings, A.J.L., Thomas, F., von Glasow, R.,
598 Wada, R., Whalley, L.K., and Whitehead, J.D.: Iodine-mediated coastal particle formation: an
599 overview of the Reactive Halogens in the Marine Boundary Layer (RHAMBLe) Roscoff
600 coastal study, *Atmos. Chem. Phys.*, 10, 2975-2999, 2010.
- 601 Metzger, A., Verheggen, B., Dommen, J., Duplissy, J., Prevot, A.S.H., Weingartner, E.,
602 Riipinen, I., Kulmala, M., Spracklen, D.V., Carslaw, K.S., and Baltensperger, U.: Evidence
603 for the role of organics in aerosol particle formation under atmospheric conditions, *PNAS*,
604 107 (15), 6646-6651, doi:10.1073/pnas.0911330107, 2010.
- 605 Minikin, A., Legrand, M., Hall, J., Wagenbach, D., Kleefeld, C., Wolff, E., Pasteur, E.C. and
606 Ducroz, F.: Sulfur-containing species (sulfate and methanesulfonate) in coastal Antarctic
607 aerosol and precipitation, *J. Geophys. Res.*, 103(D9), 10 975-10 990, 1998.

- 608 Nieminen, T., Lehtinen, K. E. J., and Kulmala, M.: Sub-10 nm particle growth by vapor
609 condensation – effects of vapor molecule size and particle thermal speed, *Atmos. Chem.*
610 *Phys.*, 10, 9773-9779, doi:10.5194/acp-10-9773-2010, 2010.
- 611 O’Dowd, C.D. and de Leeuw, G.: Marine aerosol production: a review of the current
612 knowledge, *Phil. Trans. R. Soc. A*, 365, 1753-1774, doi:10.1098/rsta.2007.2043, 2007.
- 613 O’Dowd, C.D., Hämeri, K., Mäkelä, J.M., Pirjola, L., Kulmala, M., Jennings, S.G.,
614 Berresheim, H., Hansson, H.-C., de Leeuw, G., Kunz, G.J., Allen, A.G., Hewitt, C.N.,
615 Jackson, A., Viisanen, Y., and Hoffmann, T.: A dedicated study of New Particle Formation
616 and Fate in the Coastal Environment (PARFORCE): Overview of objectives and
617 achievements. *J. Geophys. Res.*, 107(D19), 8108, doi:10.1029/2001JD000555, 2002a.
- 618 O’Dowd, C.D., Jimenez, J.L., Bahreini, R., Flagan, R.C., Seinfeld, J.H., Hämeri, K., Pirjola,
619 L., Kulmala, M., Jennings, S.G., Hoffmann, T.: Marine aerosol formation from biogenic
620 iodine emissions, *Nature*, 417, 632-636, doi:10.1038/nature00775, 2002b.
- 621 Park, J., Sakurai, H., Vollmers, K., McMurry, P.H.: Aerosol size distributions measured at
622 South Pole during ISCAT, *Atmos. Environ.*, 38, 5493-5500,
623 doi:10.1016/j.atmosenv.2002.12.001, 2004.
- 624 Pechtl, S., Lovejoy, E.R., Burkholder, J.B., and von Glasow, R.: Modeling the possible role of
625 iodine oxides in atmospheric new particle formation, *Atmos. Chem. Phys.*, 6, 505-523,
626 doi:10.5194/acp-6-505-2006, 2006.
- 627 Piel, C., Weller, R., Huke, M. and Wagenbach, D.: Atmospheric methane sulfonate and non-
628 sea salt sulphate records at the EPICA deep-drilling site in Dronning Maud Land, Antarctica,
629 *J. Geophys. Res.*, 111(D03304), doi:10.1029/2005JD006213, 2006.
- 630 Ramanathan, V., Crutzen, P.J., Kiehl, J.T., Rosenfeld, D.: Aerosols, Climate, and the
631 Hydrological Cycle, *Science*, 294, 2119-2124, 2001.
- 632 Riccobono, F., Rondo, L., Sipilä, M., Barmet, P., Curtius, J., Dommen, J., Ehn, M., Ehrhart,
633 S., Kulmala, M., Kürten, A., Mikkilä, J., Paasonen, P., Petäjä, T., Weingartner, E., and
634 Baltensperger, U.: Contribution of sulfuric acid and oxidized organic compounds to particle

- 635 formation and growth, *Atmos. Chem. Phys.*, 12, 9427-9439, doi:10.5194/acp-12-9427-2012,
636 2012.
- 637 Riipinen, I., Yli-Juuti, T., Pierce, J.R., Petäjä, T., Worsnop, D.R., Kulmala, M., and Donahue,
638 N.M.: The contribution of organics to atmospheric nanoparticle growth, *Nature Geoscience*,
639 5, 453-458, doi:10.1038/ngeo1499, 2012.
- 640 Roscoe, H.K., Jones, A.E., Brough, N., Weller, R., Saiz-Lopez, A., Mahajan, A.,
641 Schoenhardt, A., Burrows, J.P., Fleming, Z.L.: Particles and iodine compounds in coastal
642 Antarctica, *J. Geophys. Res. Atmos.*, 120, doi:10.1002/2015JD023301, 2015.
- 643 Rosenfeld, D., Andreae, M.O., Asmi, A., Chin, M., de Leeuw, G., Donovan, D.P., Kahn, R.,
644 Kinne, S., Kivekäs, N., Kulmala, M., Lau, W., Schmidt, K.S., Suni, T., Wagner, T., Wild, M.,
645 and Quaas, J.: Global observations of aerosol-cloud-precipitation-climate interactions, *Rev.*
646 *Geophys.*, 52, doi:10.1002/2013RG000441, 2014.
- 647 Saiz-Lopez, A., Mahajan, A.S., Salmon, R.A., Bauguitte, J.-B., Jones, A.E., Roscoe, H.K.,
648 and Plane, J.M.C.: Boundary Layer Halogens in Coastal Antarctica, *Science*, 317, 348-351,
649 doi:10.1126/science.1141408, 2007.
- 650 Saiz-Lopez, A., Plane, J.M.C., Baker, A.R., Carpenter, L.J., von Glasow, R., Gómez Martín,
651 J.C., McFiggans, G., and Saunders, R.W.: Atmospheric Chemistry of Iodine, *Chem. Rev.*, 112
652 (3), 1773-1804, doi:10.1021/cr200029u, 2012.
- 653 Schönhardt, A., Begoin, M., Richter, A., Wittrock, F., Kaleschke, L., Gómez Martín, J. C.,
654 and Burrows, J. P.: Simultaneous satellite observations of IO and BrO over Antarctica,
655 *Atmos. Chem. Phys.*, 12, 6565-6580, doi:10.5194/acp-12-6565-2012, 2012.
- 656 Spracklen, D. V., Carslaw, K. S., Kulmala, M., Kerminen, V.-M., Mann, G. W., and Sihto, S.-
657 L.: The contribution of boundary layer nucleation events to total particle concentrations on
658 regional and global scales, *Atmos. Chem. Phys.*, 6, 5631-5648, doi:10.5194/acp-6-5631-2006,
659 2006.
- 660 Spracklen, D. V., Carslaw, K. S., Kulmala, M., Kerminen, V.-M., Sihto, S.-L., Riipinen, I.,
661 Merikanto, J., Mann, G. W., Chipperfield, M. P., Wiedensohler, A., Birmili, W., Lihavainen,

- 662 H.: Contribution of particle formation to global cloud condensation nuclei concentrations,
663 *Geophys. Res. Lett.*, 35, L06808, doi:10.1029/2007GL033038, 2008.
- 664 Stohl, A.: Computation, accuracy and applications of trajectories-a review and bibliography,
665 *Atmos. Environ.*, 32(6), 947-966, 1998.
- 666 Stull, R.B.: *An Introduction to Boundary Layer Meteorology*, Kluwer Academic Publishers,
667 Dordrecht, Dordrecht, 175-180, 1988.
- 668 Teinilä, K., Frey, A., Hillamo, R., Tülp, H.C., and Weller, R.: A study of the sea-salt
669 chemistry using size-segregated aerosol measurements at coastal Antarctic station Neumayer,
670 *Atmos. Environ.*, 96, 11-19, 2014.
- 671 Virkkula, A., Hirsikko, A., Vana, M., Aalto, P.P., Hillamo, R., and Kulmala, M.: Charged
672 particle size distributions and analysis of particle formation events at the Finnish Antarctic
673 research station Abao, *Boreal Environ. Res.*, 12, 397-408, 2007.
- 674 Virkkula, A., Backman, J., Aalto, P. P., Hulkkonen, M., Riuttanen, L., Nieminen, T., dal
675 Maso, M., Sogacheva, L., de Leeuw, G., and Kulmala, M.: Seasonal cycle, size dependencies,
676 and source analyses of aerosol optical properties at the SMEAR II measurement station in
677 Hyttiälä, Finland, *Atmos. Chem. Phys.*, 11, 4445-4468, doi:10.5194/acp-11-4445-2011,
678 2011.
- 679 Wang, S.C. and Flagan, R.C.: Scanning Electrical Mobility Spectrometer, *Aerosol Sci.*
680 *Technol.*, 13,230-240, 1990.
- 681 Wang, J., McGraw, R. L., and Kuang, C.: Growth of atmospheric nano-particles by
682 heterogeneous nucleation of organic vapor, *Atmos. Chem. Phys.*, 13, 6523-6531,
683 doi:10.5194/acp-13-6523-2013, 2013.
- 684 Weller, R., and Lampert, A.: Optical properties and sulfate scattering efficiency of boundary
685 layer aerosol at coastal Neumayer Station, Antarctica, *J. Geophys. Res.*, 113, D16208,
686 doi:10.1029/2008JD009962, 2008.

- 687 Weller, R., Minikin, A., Wagenbach, D., and Dreiling, V.: Characterization of the inter-
688 annual, seasonal, and diurnal variations of condensation particle concentrations at Neumayer,
689 Antarctica, *Atmos. Chem. Phys.*, 11, 13243-13257, doi:10.5194/acp-11-13243-2011, 2011a.
- 690 Weller, R., Wagenbach, D., Legrand, M., Elsässer, C., Tian-Kunze, X., and König-Langlo, G.:
691 Continuous 25-years aerosol records at coastal Antarctica – 1: inter-annual variability of ionic
692 compounds and links to climate indices, *Tellus*, 63B, 901-919, doi: 10.1111/j.1600-
693 0889.2011.00542.x, 2011b.
- 694 Weller, R., Levin, I., Schmithüsen, D., Nachbar, M., Asseng, J., and Wagenbach, D.: On the
695 variability of atmospheric ^{222}Rn activity concentrations measured at Neumayer, coastal
696 Antarctica, *Atmos. Chem. Phys.*, 14, 3843-3853, doi:10.5194/acp-14-3843-2014, 2014.
- 697 Yli-Juuti, T., Nieminen, T., Hirsikko, A., Aalto, P. P., Asmi, E., Hörrak, U., Manninen, H. E.,
698 Patokoski, J., Dal Maso, M., Petäjä, T., Rinne, J., Kulmala, M., and Riipinen, I.: Growth rates
699 of nucleation mode particles in Hyytiälä during 2003–2009: variation with particle size,
700 season, data analysis method and ambient conditions, *Atmos. Chem. Phys.*, 11, 12865-12886,
701 doi:10.5194/acp-11-12865-2011, 2011.
- 702 Yu, F. and Luo, G.: Oceanic Dimethyl Sulfide Emission and New Particle Formation around
703 the Coast of Antarctica: A Modeling Study of Seasonal Variations and Comparison with
704 Measurements, *Atmosphere*, 1, 34-50, doi:10.3390/atmos1010034, 2010.
- 705 Zhang, R., Khalizov, A., Wang, L., Hu, M., and Xu, W.: Nucleation and Growth of
706 Nanoparticles in the Atmosphere, *Chem. Rev.*, 112, 1957-2011, doi:10.1021/cr2001756,
707 2012.

Table 1. Nucleation events of class I (Dal Maso et al., 2005) during austral summer 2012 and 2014: Time period during which the particle growth in the given range was observed, growth rate determined by log normal mode fitting and maximum concentration (in parenthesis) method, particle formation rate in the size range 3 nm to 25 nm (J_{3-25}), and estimated H_2SO_4 vapour concentration needed for the observed growth rate.

Date (doy 2012)	Time period	Growth rate ($nm\ h^{-1}$)	Range (nm)	J_{3-25} ($cm^{-3}\ s^{-1}$)	H_2SO_4 needed ($molec\ cm^{-3}$)
27 Jan 2012 (27)	07:00–14:00	1.9 ± 0.1 (2.5 ± 0.3)	18.7 – 33.7	0.1 ± 0.05	7.3×10^7
	11:00–18:00	1.8 ± 0.1 (2.1 ± 0.3)	6.8 – 20.2	n.d.*	6.6×10^7
23 Feb. 2012 (54)	12:00–18:00	0.6 ± 0.07 (n.d.)	4.9 – 8.9	0.1 ± 0.03	2.4×10^7
25 Feb. 2012 (56)	13:00–17:00	0.9 ± 0.07 (n.d.)	5.2 – 8.4	0.03 ± 0.01	3.3×10^7
27 Feb. 2012 (58)	11:00–18:00	1.0 ± 0.05 (1.1 ± 0.2)	11.6 – 18.5	0.06 ± 0.02	3.7×10^7
	13:00–18:00	0.9 ± 0.09 (1.0 ± 0.2)	5.2 – 9.1	0.06 ± 0.02	3.7×10^7
08 Mar. 2012 (68)	08:00–17:00	0.8 ± 0.04 (1.0 ± 0.1)	7.8 – 14.8	0.02 ± 0.01	3.2×10^7
09 Mar. 2012 (69)	14:00–19:00	0.8 ± 0.08 (1.4 ± 0.3)	5.2 – 9.1	0.08 ± 0.03	3.7×10^7
16 Mar. 2012 (76)	10:00–16:00	0.8 ± 0.1 (1.5 ± 0.6)	13.2 – 18.3	0.07 ± 0.02	3.0×10^7
	14:00–21:00	1.0 ± 0.09 (1.1 ± 0.2)	5.9 – 12.9	0.09 ± 0.03	1.8×10^7
24 Mar. 2012 (84)	15:00–19:00	0.5 ± 0.05 (n.d.)	4.1 – 6.1	0.02 ± 0.01	2.7×10^7
06 Feb. 2014	14:00–19:00	$0.4\pm 0.2^\ddagger$ (n.d.)	8.8 – 11.3 [‡]	n.d. [†]	1.5×10^7
24 Mar. 2014	11:00–18:00	0.5 ± 0.1 (n.d.)	14.5 – 16.6	n.d. [†]	1.7×10^7

* n.d. = not determined

[‡] measured with the long DMA (TSI model 3081) with enhanced uncertainty below 10 nm

[†] particle formation rate not determined due to higher cut-off of the SMPS used during this period

Table 2. Comparison of selected meteorological and aerosol light scattering parameters as well as ionic composition of the aerosol (all items in mean \pm std) during days with NPF as characterized in Table 2 and non-event days. The comparison is restricted to the summer months (January through March).

parameter	NPF event	non-event
relative humidity (%)	77.9 \pm 4.7	82.4 \pm 5.1
p(H ₂ O) (hPa)	262 \pm 98	281 \pm 100
$\sigma_{\text{sp}}(450)$ (Mm ⁻¹)	2.30 \pm 0.9	3.20 \pm 2.2
$\sigma_{\text{sp}}(550)$ (Mm ⁻¹)	1.65 \pm 0.7	2.50 \pm 1.9
$\sigma_{\text{sp}}(700)$ (Mm ⁻¹)	1.30 \pm 0.5	2.00 \pm 1.5
$\alpha_{\text{sc}}(450-550)$	1.8 \pm 0.2	1.4 \pm 0.2
$\alpha_{\text{sc}}(450-700)$	1.4 \pm 0.2	1.3 \pm 0.2
$\alpha_{\text{sc}}(550-700)$	1.2 \pm 0.2	1.3 \pm 0.3
MSA ⁻ (ng m ⁻³)	109 \pm 54	132 \pm 100
nss-SO ₄ ²⁻ (ng m ⁻³)	225 \pm 67	274 \pm 160
Na ⁺ (ng m ⁻³)	45 \pm 19	79 \pm 130
NH ₄ ⁺ (ng m ⁻³)	6.6 \pm 3	12.5 \pm 11

Figure captions

Figure 1. Time series of the measured particle size distribution $dN/d\log D_p$ (cm^{-3}) on a logarithmic scale (color code to the right of the contour plot) of NPF events around 27 January 2012 showing a growing nucleation and Aitken mode (a), corresponding CP concentration (black line) and particle concentrations between 3 nm and 25 nm (UCP_{3-25} , red line) (b), wind velocity (red line), wind direction (black line) and Ri_B (blue line) (c), light scattering coefficients σ_{sp} at 450 nm, 550 nm, and 700 nm (blue, green and red lines) as well as UV radiation at wavelengths between 300 nm and 370 nm (purple line) (d), aerosol mass m_p derived from SMPS measurements assuming a density of 1.8 g cm^{-3} , as well as MSA^- , nss-SO_4^{2-} , Na^+ , and NH_4^+ concentrations derived from daily aerosol samples (red lines mark the time of filter exchange) (e).

Figure 2. Detailed presentation of the NPF event around 27 January 2012 with a linear $dN/d\log D_p$ (cm^{-3}) scale as z-axis, based on hourly mean SMPS data recorded with 64 channel resolution. The lower panel shows exemplarily six log-normal distribution fits through size distributions measured at 27 January between 12:00 and 17:00. The mode mean diameters (in nm) are noted next to the respecting modal maxima.

Figure 3. Time series of particle size distribution $dN/d\log D_p$ (cm^{-3}) measured during winter 2014 (12 August through 27 September, logarithmic color code to the right of the contour plot) (a), CP concentration (b), wind velocity (red line) and wind direction (black line) (c). The yellowish shaded areas in (c) mark stormy weather conditions associated with snow drift.

Figure 4. Mean size distribution (red line) and range of geometric standard deviation (grey envelope) during both winter particle nucleation events (15/16 August and 21 September 2014), as well as for typical winter day without nucleation (18 August 2012).

Figure 5. Five-day back trajectories based on 3D wind fields for the period 26 January 2012 through 28 January 2012: Horizontal advection pattern (a) and vertical profiles (b). Trajectories which arrived around the main NPF events (noon on 26 and 27 January 2012) are plotted as bold lines.

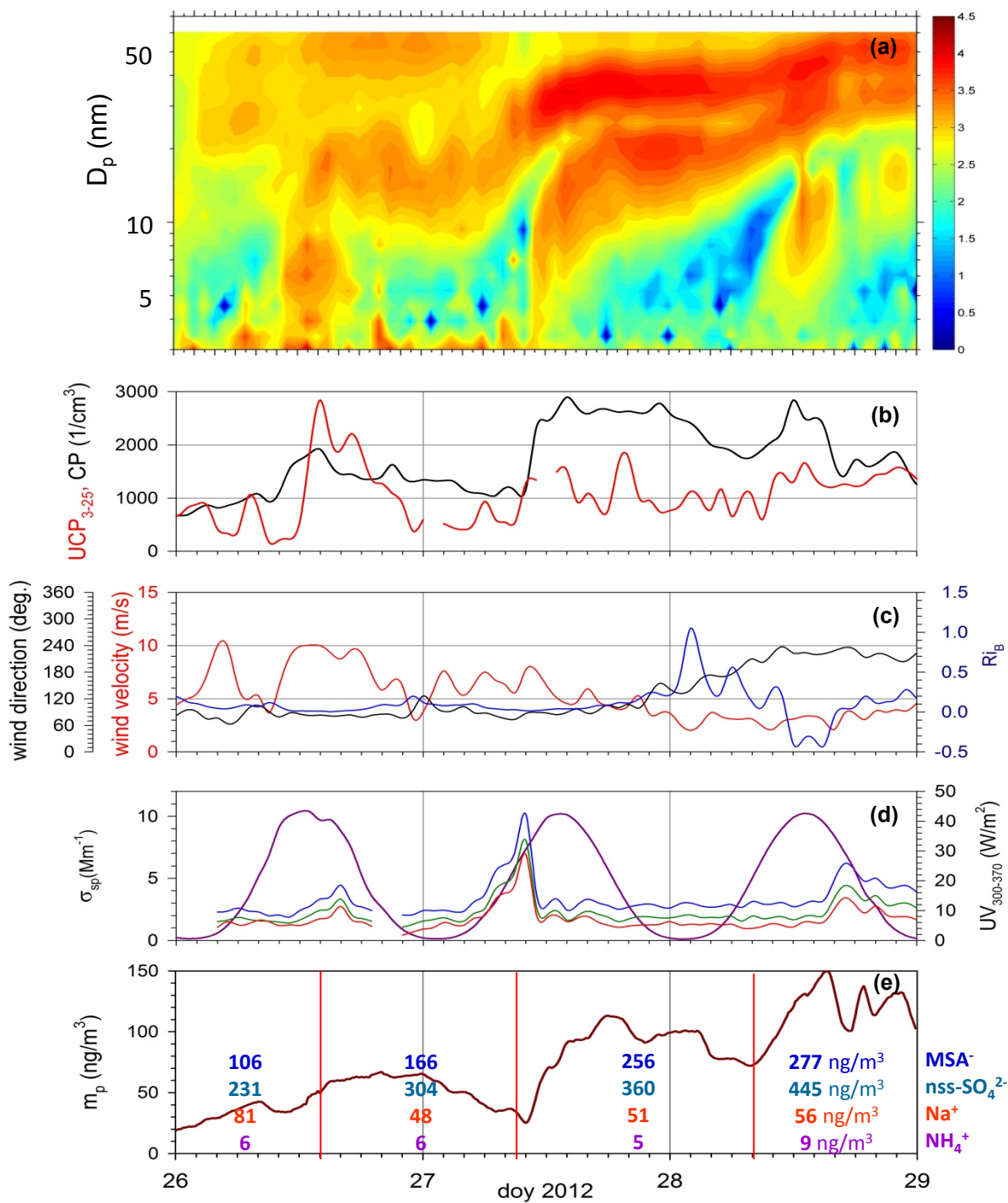


Figure 1

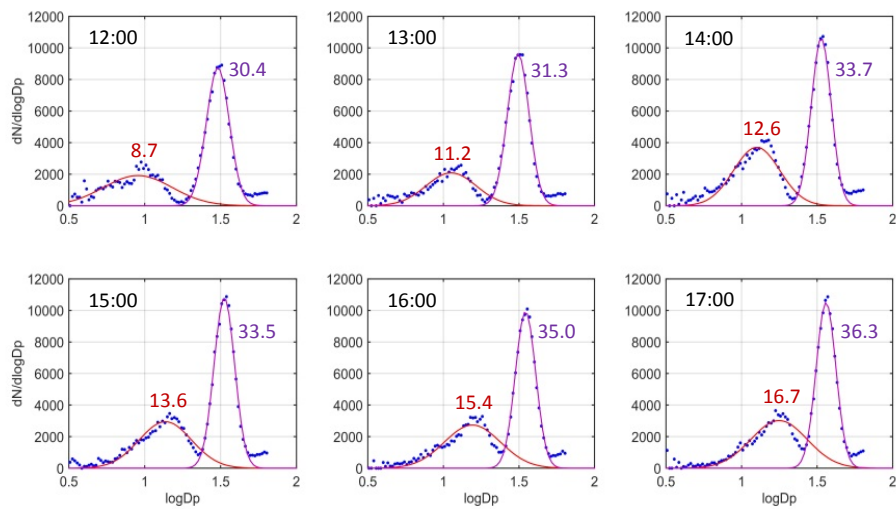
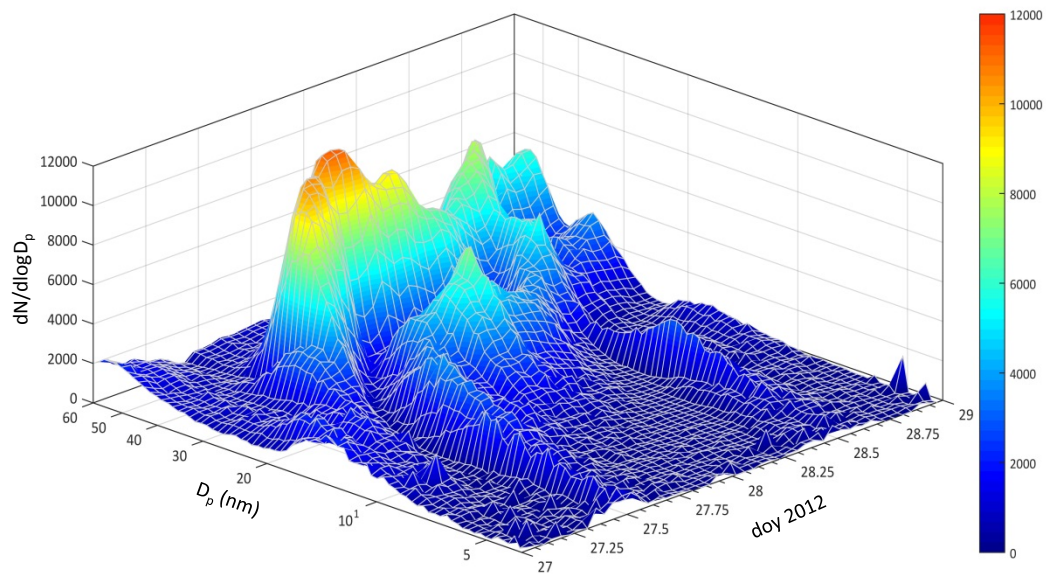


Figure 2

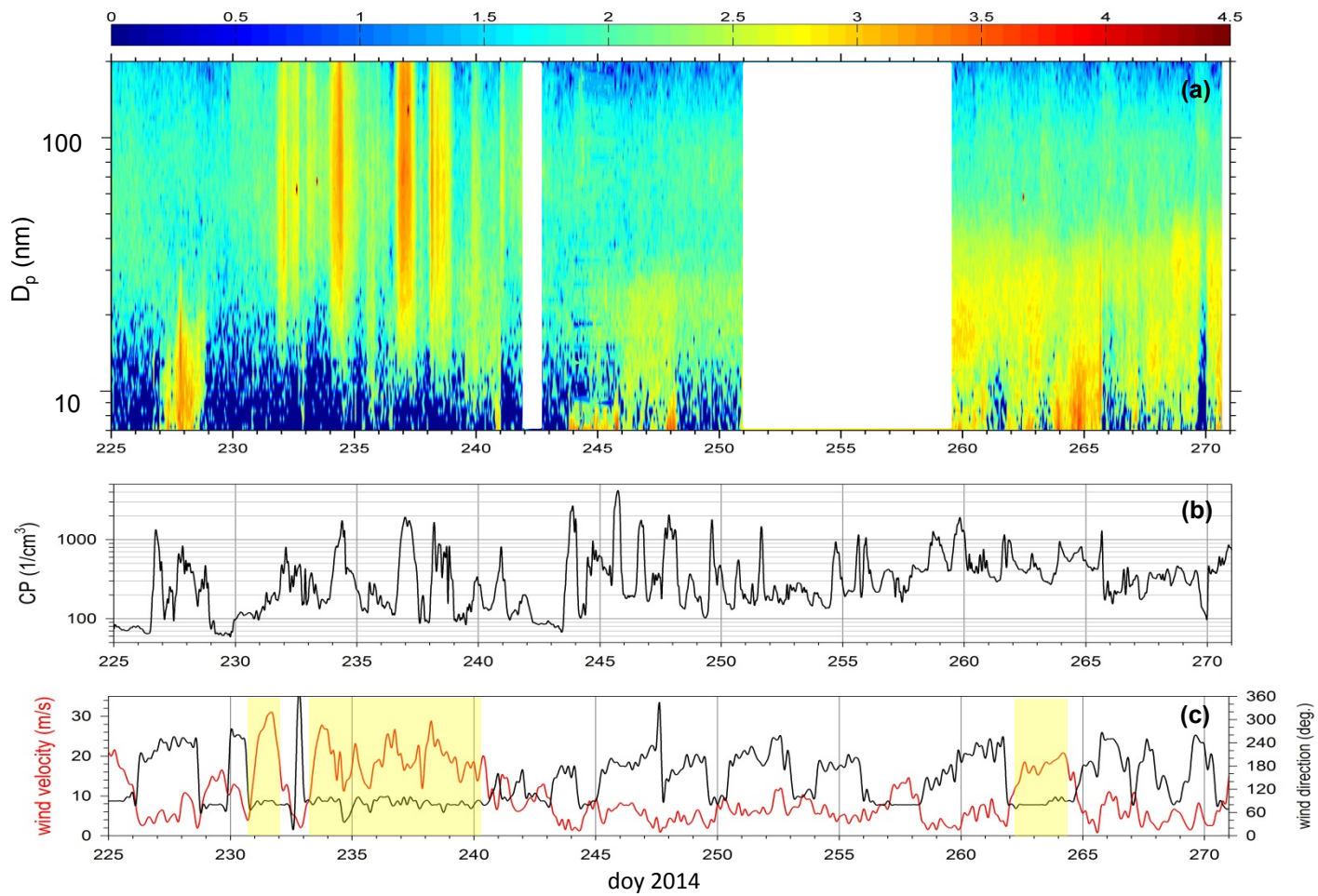


Figure 3

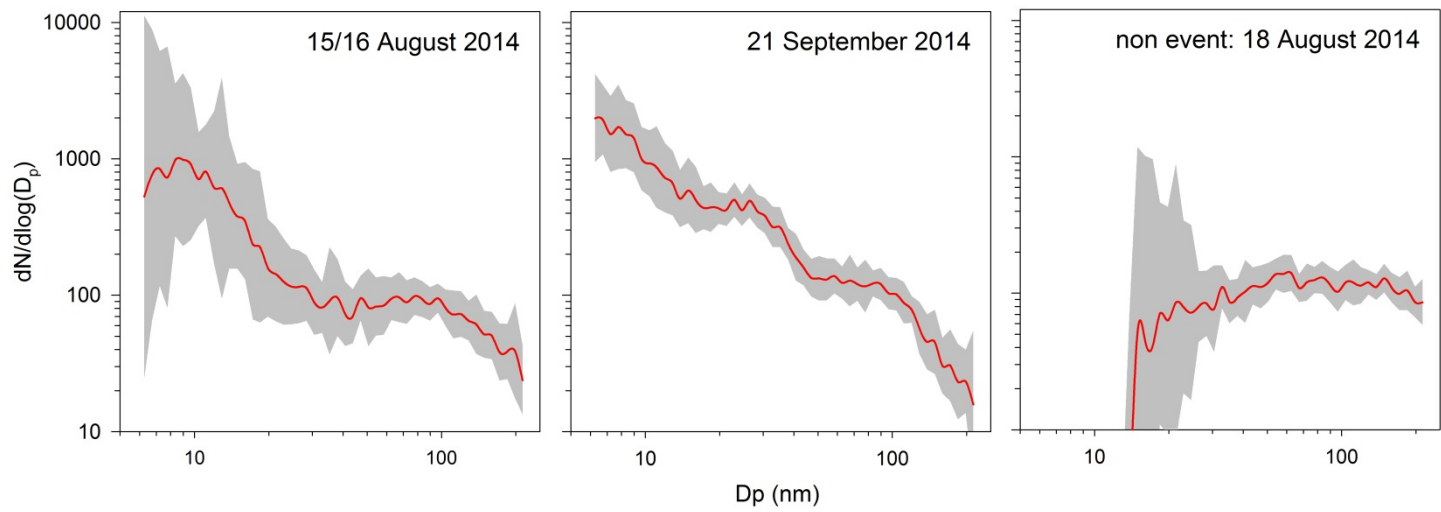


Figure 4

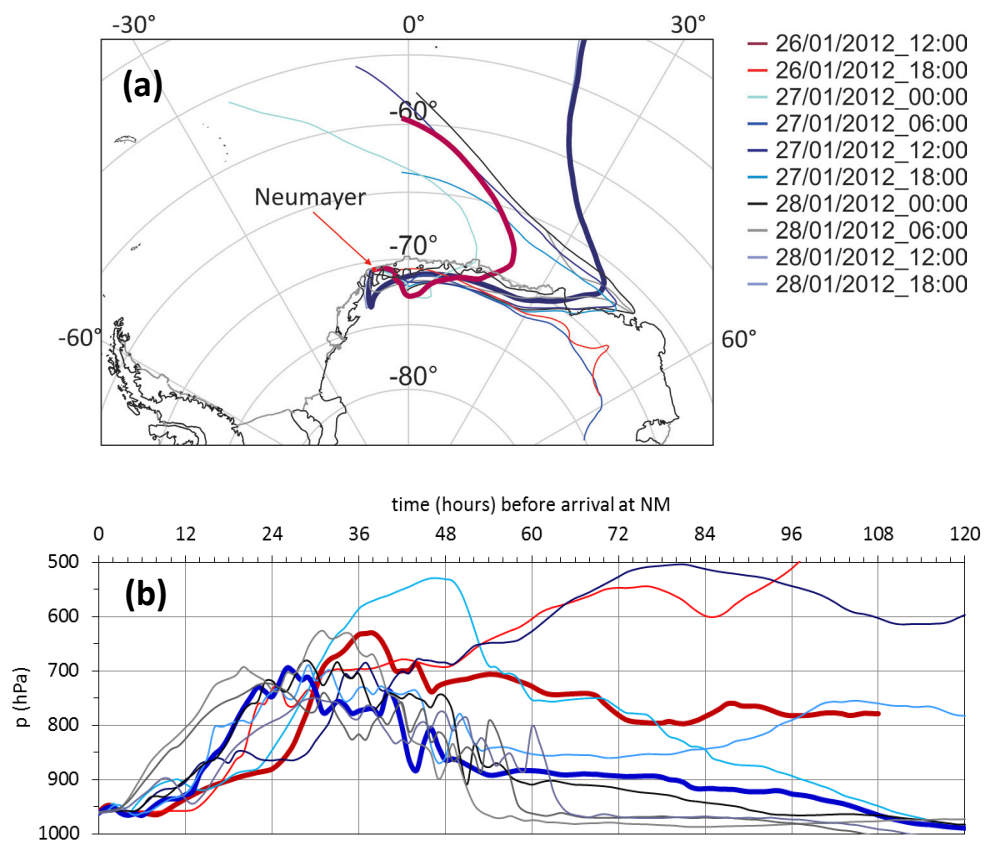


Figure 5